Pu-Ste Liu,[1] Yi-Wei Lin,[1] Bomi Lee,[1] Shelly K. McCrady-Spitzer,[2] James A. Levine,[2] and Li-Na Wei[1]

Reducing RIP140 Expression in Macrophage Alters ATM Infiltration, Facilitates White Adipose Tissue Browning, and Prevents High-Fat Diet–Induced Insulin Resistance

Adipose tissue macrophage (ATM) recruitment and activation play a critical role in obesity-induced inflammation and insulin resistance (IR). The mechanism regulating ATM activation and infiltration remains unclear. In this study, we found receptor interacting protein 140 (RIP140) can regulate the dynamics of ATM that contribute to adipose tissue remodeling. A high-fat diet (HFD) elevates RIP140 expression in macrophages. We generated mice with RIP140 knockdown in macrophages using transgenic and bone marrow transplantation procedures to blunt HFD-induced elevation in RIP140. We detected significant white adipose tissue (WAT) browning and improved systemic insulin sensitivity in these mice, particularly under an HFD feeding. These mice have decreased circulating monocyte population and altered ATM profile in WAT (a dramatic reduction in inflammatory classically activated macrophages [M1] and expansion in alternatively activated macrophages [M2]), which could improve HFD-induced IR. These studies suggest that reducing RIP140 expression in monocytes/macrophages can be a new therapeutic strategy in treating HFD-induced and inflammation-related diseases.

Macrophages are found in all tissues and, when activated by various signals, mainly function in innate immunity such as to regulate inflammatory responses. Functionally, macrophages are binarily classified into classically activated (M1) and alternatively activated (M2) states (1). Molecular determinants for certain specific macrophage phenotypes have been investigated (2,3), and different tissue macrophages have diverse gene expression and transcriptional profiles (4). In the white adipose tissue (WAT), both the number and state of activation of adipose tissue macrophages (ATMs) can be altered by various factors and usually reflect the WAT's metabolic state (5). For instance, in a high-fat diet (HFD)-induced obesity model, ATM populations dramatically expand from a healthy 10–15% of stromal cells (mostly in the M2 state that is suggested to maintain the homeostasis and insulin sensitivity of the adipose tissue) to a 45–60% representation (mostly due to increased infiltration/recruitment of inflammatory monocytes that turn into M1 macrophages) (6). This indicates a state of chronic low-grade inflammation of the WAT. Concurrently, WAT enlarges and remodels to accommodate the demand in fat storage, and the substances released from these enlarged white adipocytes, especially fatty acids, further worsen the degree of inflammation, resulting in a vicious cycle of chronic inflammation in the WAT and leading to insulin resistance (IR) (7,8).

M2 ATMs predominate in lean mice, and obesity induces the accumulation of M1 ATMs, leading to a proinflammatory state (9). Recent studies have indicated that certain populations of circulating monocytes may be more susceptible to recruitment to AT (1). In addition, other AT-derived molecules, such as chemokines and inflammatory mediators, have also been evaluated for their roles in recruiting and activating these monocytes/ATMs (10). The mechanism behind the shift in ATM phenotypes may be related to changes in circulating monocyte populations and/or differential recruitment of various monocyte subtypes to AT. In mice, $CCR2^+Ly6C^+$ monocytes are preferentially recruited to the sites of tissue inflammation and precursors of classically activated M1 macrophages. In contrast, $CCR2^-Ly6C^-$ monocytes appear to be regulated by different stimuli and may play a role in patrolling noninflamed tissues and give rise to resident tissue macrophages (11,12). Importantly, monocytes are generally expanded with the progression of obesity, suggesting that these monocytes may present inflammatory mediators of obesity-induced inflammation. Which monocyte population traffics to AT in HFD-induced obesity is not well defined (13).

Receptor interacting protein 140 (RIP140; also known as Nrip1) is a wide-spectrum transcription coregulator (14,15) and highly expressed in various cell types, including adipocytes (16), neurons, and cells in the monocyte–macrophage lineage (17). In differentiating adipocytes, RIP140 functions as a corepressor for heterochromatinization of gene loci that are to be silenced in mature adipocytes (18); in fully expanded adipocytes, RIP140 undergoes sequential posttranslational modifications and translocates to the cytoplasm to participate in cytosolic events such as GLUT4 vesicle transport, adiponectin vesicle transport, and lipolysis (19,20). A recent study (21) indicated that knockout of RIP140 in mice caused browning within white fat depots. RIP140 blocked the browning program through repression of the expression of brown AT (BAT) and beige genes and a triacylglycerol futile cycle in WAT. In M1 macrophages, RIP140 contributes to their inflammatory response by acting as a coactivator of nuclear factor-κB and regulates endotoxin tolerance (22,23). We also found that an HFD elevates RIP140 expression in peritoneal macrophages (PMs), which activates tumor necrosis factor-α and interleukin (IL)-1β expression and enhances macrophages' inflammatory potential, thereby contributing to increased susceptibility to septic shock (17). However, whether RIP140 plays a functional role in monocytes and ATMs in obesity is unknown.

In order to examine whether RIP140 is involved in ATM homeostasis, we generated transgenic mice with RIP140 knockdown (KD) in monocytes/macrophages, as well as using bone marrow transplantation (BMT) procedures. We detected a browning phenotype in AT of these mice in which RIP140 was reduced only in monocytes/macrophages. This phenotype was associated with increased thermogenesis and energy expenditure, as well as improved insulin sensitivity particularly under HFD. This was also correlated with reduced M1 circulating monocytes and their recruitment into WAT of these animals.

RESEARCH DESIGN AND METHODS

Animal

All studies were carried out using male C57Bl/6 mice from The Jackson Laboratory and maintained in the animal facility of University of Minnesota and approved by the University of Minnesota Institutional Animal Care and Use Committee. MφRIP140KD mice were generated as previously described. Mice were fed a normal diet (ND) containing 18% calories from fat and undetectable cholesterol (2018; Harlan Teklad, Madison, WI) or an HFD containing 60% calories from fat and 345 mg cholesterol/kg (F3282; Bio-Serv, West Chester, PA).

Glucose Tolerance and Insulin Tolerance Tests

Glucose tolerance test (GTT) or insulin tolerance test (ITT) was performed after overnight fasting. After baseline blood collection, mice were i.p. injected with D-glucose (2 g/kg) or insulin (0.75 units/kg). Blood glucose levels at indicated time points were measured with a standard glucometer.

Metabolic Measurement

Indirect calorimetry was performed at 12 weeks of age (n = 6 mice/group) to measure oxygen consumption (vO_2). Animals were trained to habituate metabolic cages 3 days before measurement and maintained in a 12-h light/dark cycle in individual chambers with free access to chow and water. vO_2 measurement was recorded every 4 min for 2 days and normalized to body mass using Oxymax (Columbus Instrument, Columbus, OH). Food intake was monitored by weighing food hoppers.

Insulin Signaling

Mice were fed an HFD for 15 weeks and overnight fasted the night before. Mice were intraperitoneally administered with/without insulin. Ten minutes later, visceral WAT (vWAT) was collected for extracting protein.

PM Isolation

Mice were i.p. injected with 4% thioglycollate and killed 4 days later. PMs were collected by peritoneal lavage with 10 ml 1× PBS and plated with DMEM plus 10% FBS. Nonadherent cells were removed 24 h later. Adherent cells were 90% macrophages.

Conditioned Medium of BM-Derived Macrophage Cells

BM-derived macrophage (BMDM) cells were harvested from femurs and tibias of 8-week-old mice and plated at 1×10^7 cells/plate in DMEM plus 10 mg/mL macrophage colony-stimulating factor plus 10% FBS for 8 days differentiation prior to use. Differentiated BMDMs were switched to 10% FBS-containing medium and stimulated with IL-4 for 12 h. IL-4 medium is then removed, and BMDM cells continue to be cultured for 12 h for the collection of conditioned medium (CM).

BMT

BM cells were labeled with PKH26 (Red Fluorescent Cell Linker Mini Kit; Sigma-Aldrich) in vitro and retro-orbitally injected into lethally irradiated recipient WT mice with a dose of 10^7 cells. Recipient mice were allowed 4 to 5 weeks to reconstitute their hematopoietic systems with wild-type (WT) or RIP140KD BM cells. PKH26 expression in BM cells of the recipient mice was monitored to determine BMT efficiency.

Plasma Measurements

Blood was collected at the time of sacrifice, and fasting plasma insulin level in mice unfed for 16 h was measured using an insulin ELISA kit (catalog number EZRMI-13K; Millipore). Plasma adiponectin levels were measured using an adiponectin ELISA kit (catalog number EZMADP-60K; Millipore). Total cholesterol levels were determined using a cholesterol assay kit (10007640; Cayman Chemical Company). Serum triglycerides and free fatty acids were measured using an L-type TG H kit and NEFA C kit (Wako Chemicals).

Isolating Stromal Vascular Fraction of WAT

WAT was minced and digested with type II collagenase (Sigma-Aldrich), filtered through a 100-µm nylon sieve, and centrifuged at 500 × *g* to separate floating adipocytes from the stromal vascular fraction (SVF) pellet. SVF was treated with an RBC lysis buffer (Sigma-Aldrich).

In Vitro Adipocyte Differentiation

SVF was isolated and differentiated for 8 days as following: preadipocytes were isolated and cultured in medium containing 10% FBS, 0.5 mmol/L isobutylmethylxanthine, 0.125 mmol/L indomethacin, 1 µmol/L dexamethasone, 850 nmol/L insulin, 1 nmol/L T3, and 1 µmol/L rosiglitazone for 2 days. Cells were switched to a maintenance medium containing 10% FBS, 850 nmol insulin, and 1 nmol/L T3 for 6 days. Control- or MφRIP140KD BMDM-CM was added on day 2 in adipocyte differentiation for a total of 6 days. Following adipocyte differentiation, on day 8, cells were incubated with 10 µmol/L isoproterenol for 4 h for stimulate thermogenesis.

Reagents

Anti-phosphorylated insulin receptor substrate-1 (IRS-1; Ser[307]), anti-Akt, anti–phosphorylated Akt (Ser[473]), anti–β-actin (Santa Cruz Biotechnology), and anti–IRS-1 (Upstate Biotechnology) were used in Western blotting. Rabbit anti-CD137 (Abcam), rabbit anti-TMEM26 (Imgenex), rabbit anti–UCP-1 (Abcam), and rat antiperilipin A (Abcam) were used for immunofluorescence.

RNA Isolation and Gene Expression Analyses

Total RNA was isolated using TRIzol (Invitrogen). Reverse transcription of 2 µg RNA was performed with a High-Capacity cDNA Reverse Transcription Kit containing RN-ase Inhibitor (Applied Biosystems). Quantitative real-time PCR (qPCR) was performed as described previously. Each gene-expression experiment was performed in triplicate. Primer sequence is available upon request.

Mitochondrial DNA Content

Genomic DNA was isolated from vWAT using the DNeasy Blood & Tissue Kit (Qiagen), and mitochondrial DNA (mtDNA) copy numbers were determined by qPCR using primers specific for mtDNA-encoded genes (CytB) and nuclear-encoded genes (H19). Relative mtDNA were measured and calculated by normalizing CytB expression level to H19 level.

Immunohistochemistry

Tissues samples were fixed, embedded in paraffin, and sectioned. A morphometric study was performed in vWAT sections stained with hematoxylin and eosin.

Flow Cytometry

Cell-surface antigens were blocked with Fc Block (20 µg/mL; BD Biosciences) and stained with fluorophore-conjugated antibodies or isotype control antibodies for 1 h. Fluorophore-conjugated primary antibodies used in these studies are F4/80-FITC, CD11c-phycoerythrin, and CD206–Alexa Fluor 647 (eBioscience); CD45-phycoerythrin (BD Biosciences), CD19-FITC (BD Biosciences), CD4-PerCP (eBioscience), CD3e-FITC (eBioscience), CD115–Alexa Fluor 488 (BD Biosciences), and Ly6G–Alexa Fluor 647 (BD Biosciences). After incubation with antibodies, cells were washed and centrifuged at 500 × *g* for 5 min, resuspended in 1 mL washing buffer, and analyzed on an FACSCalibur using FlowJo 10.0.6 software.

Statistical Analysis

Experiments were performed at least twice, and results were presented as means ± SD. Comparisons between groups were made by unpaired two-tailed Student *t* tests or one-way and two-way ANOVA. *P* values of ≤0.05 were considered statistically significant (*$P < 0.05$; **$P < 0.01$; ***$P < 0.001$).

RESULTS

RIP140 Expression in ATM Is Elevated by HFD Feeding, and Lowering RIP140 Expression in Monocytes/Macrophages Improves HFD-Induced IR

To first examine the effects of HFD on the expression of RIP140 in macrophages, particularly ATMs, we collected ATMs from mice fed an ND or HFD for 3 or 15 weeks and determined RIP140 mRNA levels. As shown in Supplementary Fig. 1*A*, the RIP140 mRNA level in ATM is significantly elevated in the HFD-fed mice as compared with the ND-fed mice. To validate the functional role of RIP140 in monocytes/macrophage in vivo, we used a monocyte/macrophage-specific promoter, CD68 (24), to express RIP140-specific inhibitory short hairpin RNAs (23) that mimic endogenous microRNAs to generate monocyte/macrophage-specific KD of RIP140 in transgenic mice (MφRIP140KD). We systemically analyzed two MφRIP140KD mouse lines (KD-1 and -2) for which issue-specific KD efficiency was similar in PMs, BMDMs, and ATMs (Supplementary Fig. 1*B*). Both lines also exhibited similar metabolic features. MφRIP140KD mice are healthy and fertile, resist HFD-induced weight gain

and systemic IR (Fig. 1A and B), and have superior metabolic profiles in such parameters as fasting glucose level, fasting insulin level, serum adiponectin, cholesterol levels, free fatty acid, and triglycerides (Fig. 1C). Consistently, in vWAT, proinflammatory adipokine mRNA levels are significantly lower, while adiponectin mRNA levels are much higher for the MφRIP140KD mice (Fig. 1D). Also, the typical suppression (under HFD) of insulin-stimulated Akt-IRS activation in vWAT is abolished in the MφRIP140KD mice (Fig. 1E). According to these metabolic measures, we conclude that MφRIP140KD mice are healthy and resist HFD-induced systemic IR and adipose inflammation.

Enhanced vWAT Browning in HFD-Fed MφRIP140KD Mice

We conducted gross anatomical examination and found that typical expansion of WAT depots after a HFD feeding was reduced in MφRIP140KD mice for both inguinal WAT (iWAT) and vWAT (Fig. 2A). HFD-induced liver weight gain was also reduced in MφRIP140KD mice (data not shown). Interestingly, there was no apparent difference in other organs including interscapular BAT, muscle, and bone (not shown). Because the most profound change was detected in WAT depots, we then focused our attention to characterize vWAT and iWAT. It appears that the vWAT of MφRIP140KD mice has multilocular fat cells and shows no adipocyte enlargement even after 15 weeks of HFD feeding (Fig. 2B). Consistently, markers of brown fat (UCP-1) and beige fat (TMEM26 and CD137) are evident in the vWAT sections of MφRIP140KD mice even after HFD feeding (Supplementary Fig. 2A); furthermore, mRNA levels of brown adipogenic markers (Pgc-1α, Ucp-1, and Prdm16) (25) and beige fat markers (Tmem26, Cd137, and Tbx 1) (26) are elevated in MφRIP140KD mice, and their vWAT contains significantly more mitochondria, consistent with increased mitochondrial activity markers (Fig. 2C and D). UCP-1 protein level is also elevated in vWAT of MφRIP140KD mice as compared with WT mice (Supplementary Fig. 2B). Interestingly, the expression of estrogen-related receptor γ, but not estrogen-related receptor α, is increased in the MφRIP140KD mice (data not shown). As in vWAT, iWAT of MφRIP140KD mice readily harvests multilocular fat cells (Supplementary Fig. 3A) and expresses higher levels of brown fat (Ucp-1, Pgc-1a, and Prdm16) and beige fat (Tmem26, Cd137, and Tbx1) markers under an ND (Supplementary Fig. 3B and C). But unlike vWAT, iWAT has no further increase in browning under HFD. While UCP-1 expression is readily high in the BAT of both WT and MφRIP140KD mice under ND, there is no further increase in browning in the BAT of MφRIP140KD mice under HFD (Supplementary Fig. 3D–F). These data show that the most dramatic change in MφRIP140KD mice is the browning of vWAT, particularly after an HFD feeding. We further examined whether CM of RIP140 KD macrophages could directly cause WAT browning. We collected WT and RIP140 KD macrophage CM to culture preadipocytes collected from vWAT depots

of WT mice for in vitro adipocyte differentiation. As shown in Fig. 2E, RIP140 KD macrophage CM indeed enhances all the markers tested that are indicative of browning, such as Ucp-1, Pgc-1α, Cidea, Dio, Acsl, and Acoxl. It has been reported that cold stress or IL-4 induction can enhance M2 macrophage polarization to produce catecholamines in BAT and WAT (27). We found that MφRIP140KD ATM expresses higher levels of tyrosine hydroxylase (TH), the rate-limiting enzyme in catecholamine synthesis (Fig. 2F, left panel), and that RIP140 KD also enhances TH mRNA level in macrophage stimulated with IL4 (Fig. 2F, right panel). We then investigated whether RIP140 KD mice would alter their energy expenditure. As shown in Fig. 2G, HFD-fed MφRIP140KD mice indeed have a higher level of energy expenditure (vO$_2$ consumption) in both the dark and light phases. As shown in Fig. 2H, food uptake is not significantly altered in RIP140KD mice. Accordingly, we conclude that MφRIP140KD mice have dramatically altered their vWAT, indicative of browning that might be caused by factors secreted by RIP140 KD macrophages. These animals resist typical chronic HFD-induced vWAT remodeling and adipose inflammation.

The promoter used to drive the short hairpin RNA, CD68, is most active in the monocyte–macrophage lineage, with negligible activity in other immune cells such as eosinophil, neutrophils, T, and B cells (Supplementary Fig. 1C). To further rule out potential effects from other non-macrophage cells and/or potential developmental factors, we used BMT to generate MφRIP140KD only in the adult stage and named these BM–restricted RIP140 KD animals "KD→WT." We then analyzed the vWAT of these KD→WT animals. Hematoxylin and eosin histology reveals that the vWAT of KD→WT mice apparently also contains multilocular fat cells (Fig. 3A), with similar elevation in brown fat (UCP-1) and beige fat (TMEM26) markers, particularly after HFD feeding (Supplementary Fig. 4). Consistently, mRNA levels of brown adipogenic (Pgc-1α, Ucp-1, and Prdm16) and beige fat (Tmem26, Cd137, and Tbx1) markers (Fig. 3B), mitochondria number (Fig. 3C), mitochondrial activity markers (Fig. 3D), and TH levels (Fig. 3E) are all significantly increased in the vWAT of KD→WT mice under an HFD. Further, KD→WT mice gain less weight (Fig. 3F) and exhibit better systemic insulin sensitivity (Fig. 3G) and superior serum metabolic parameters such as fasting glucose level, fasting insulin level, serum adiponectin, cholesterol, free fatty acid, and triglyceride levels (Fig. 3H) as compared with WT→WT mice under an HFD. KD→WT mice also have a higher level of energy expenditure (vO$_2$ consumption) in both the dark and light phases (Fig. 3I). As shown in Fig. 3J, food uptake is similar between the two types of BMT mice.

These results confirm that reducing RIP140 levels in macrophage either from birth or during adult stages reduces adipose inflammation, facilitates vWAT browning, and improves systemic insulin sensitivity in mice under an HFD.
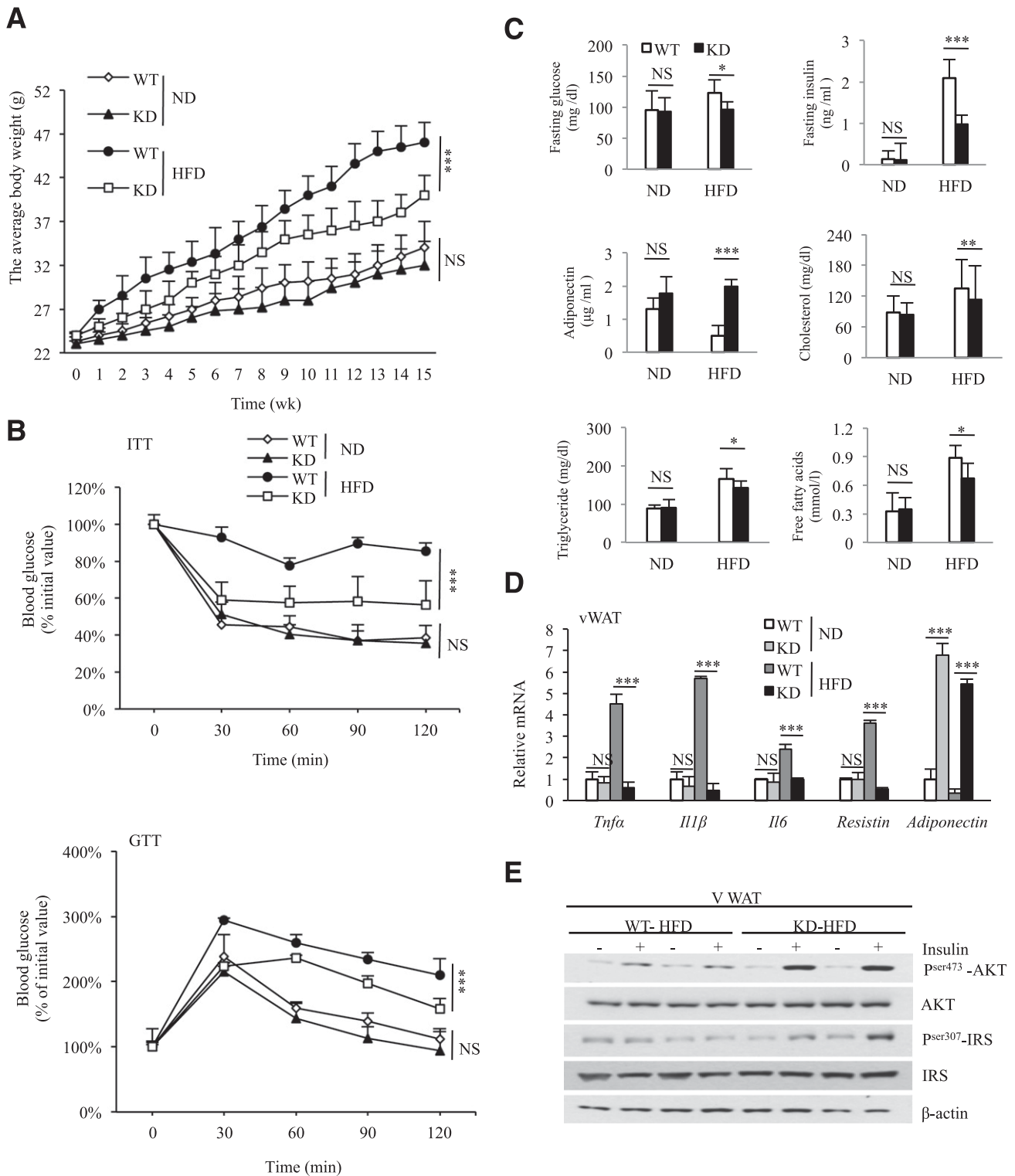
Figure 1—MφRIP140KD mice exhibit improved metabolic phenotypes. *A*: The average body weight of WT and MφRIP140KD (KD) mice fed an ND or HFD for 15 weeks. *B*: ITT and GTT determined after 15 weeks of ND or HFD feeding. *C*: Serum insulin, glucose, adiponectin, cholesterol, free fatty acid, and triglyceride levels in ND- or HFD-fed WT and KD mice. *D*: qPCR results showing mRNA levels of pro- and anti-inflammatory cytokines in the vWAT of ND- or HFD-fed WT and KD mice. *E*: Insulin signaling components in ND- or HFD-fed WT and KD adipose tissues. For *A* and *B*, two-way ANOVA test was performed. For *C* and *D*, Student test was used. All experiments were performed three times and presented as mean ± SD; *n* = 5 to 6 mice/group. *$P < 0.05$; **$P < 0.01$; ***$P < 0.001$.
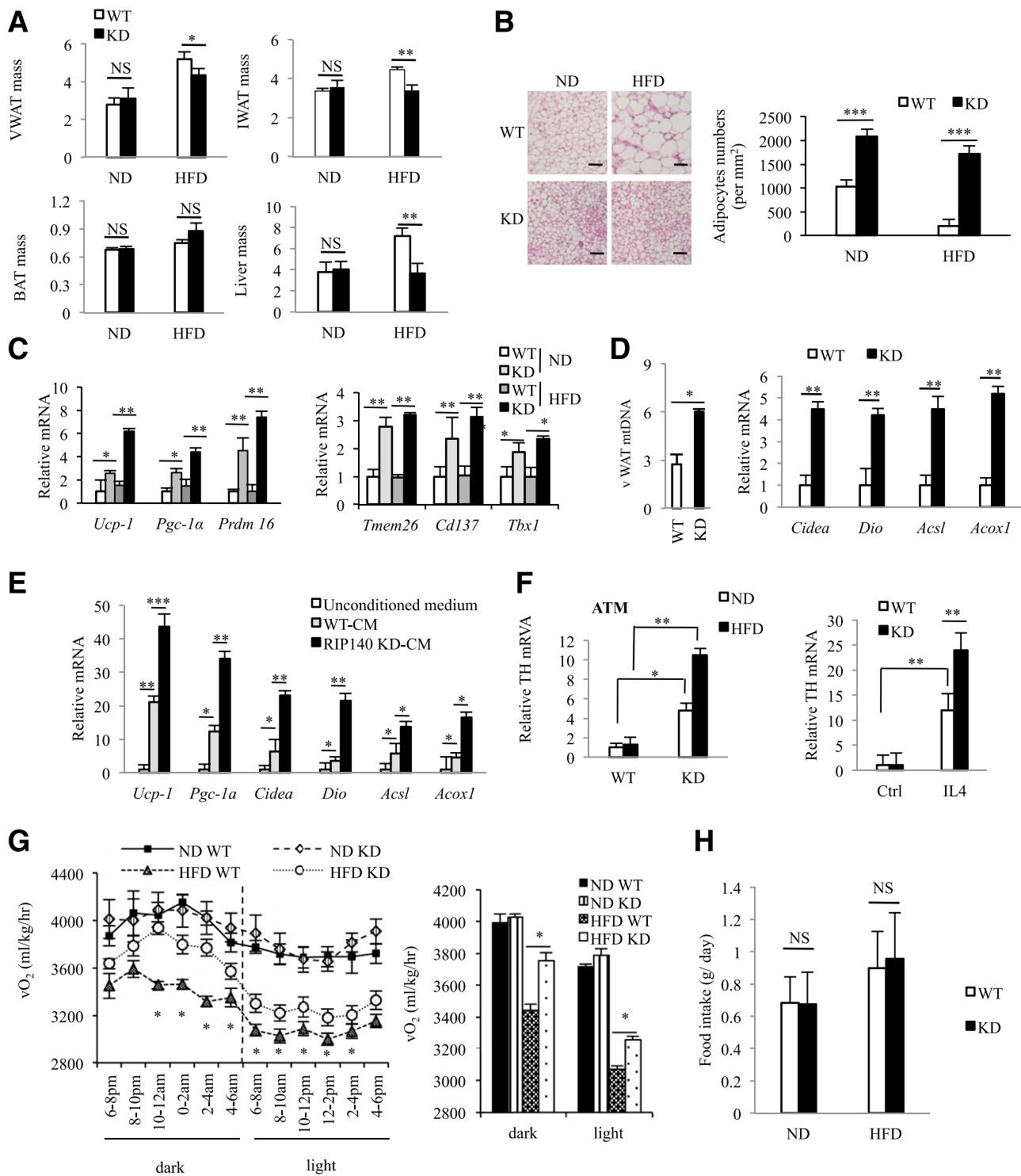
Figure 2—MφRIP140KD mice show browning in vWAT. *A*: Body weight–normalized iWAT, vWAT, and BAT tissue mass (WT: *n* = 6; KD: *n* = 6). *B*: *Left*, histological staining of vWAT. Scale bars, 200 μm. *Right*, WT and KD mice were fed an ND or HFD for 15 weeks. Sections of vWAT were stained with hematoxylin & eosin, and adipocytes were counted and presented as numbers per millimeter. *C*: qPCR results of mRNA levels in brown (*left*) and beige (*right*) fat markers in vWAT. *D*: mtDNA content and mitochondrial activity markers in vWAT. *E*: In vitro adipocyte differentiation using untreated (unconditioned medium), CM of WT, or RIP140 KD macrophage. *F*: *Left*, qPCR of relative TH mRNA levels in ATM of vWAT. *Right*, qPCR of relative TH mRNA levels in macrophages from WT or RIP140 KD, with or without IL-4 treatment. *G*: Analyses of energy expenditure of WT and KD mice. vO₂ consumption was measured in the dark and light phases as described in RESEARCH DESIGN AND METHODS (WT: *n* = 12; KD: *n* = 12). *H*: Food intake was monitored and normalized to body weight. For *A–F* and *H*, Student test was used and presented as mean ± SD. For *G*, Student test was used and presented as mean ± SEM. *P < 0.05; **P < 0.01; ***P < 0.001.
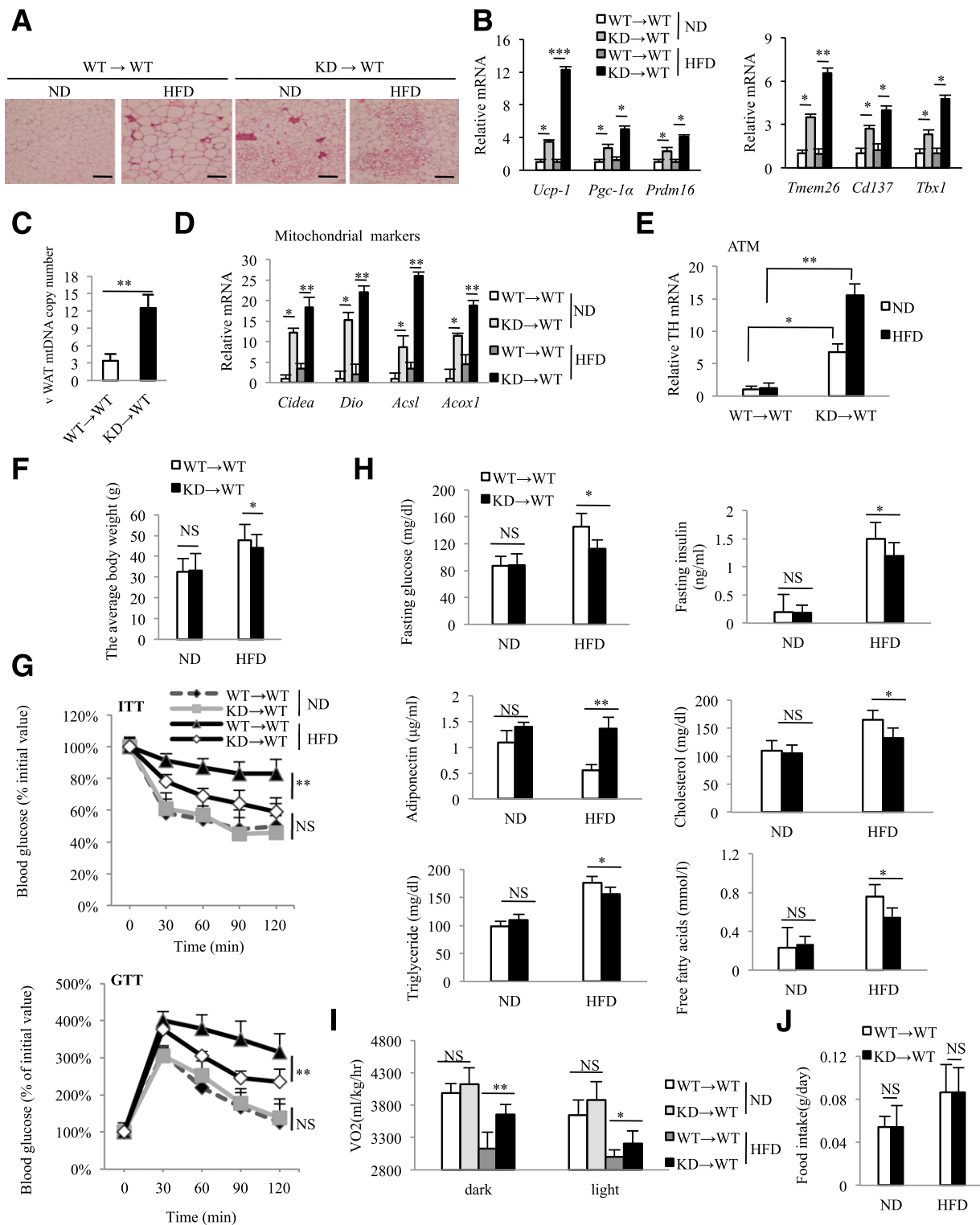
Figure 3—Induction of browning phenotype in MφRIP140KD produced with BMT. A: After BMT reconstitution, WT→WT and KD→WT mice were fed an ND or HFD for 15 weeks. Histological staining of vWAT. Scale bars, 200 μm (WT: n = 6; KD: n = 6). B: qPCR data showing mRNA levels of brown and beige fat markers in vWAT (WT: n = 6; KD: n = 6). mtDNA content (C) and mitochondrial activity markers (D) in vWAT were detected. E: qPCR of relative TH mRNA levels in ATMs of vWAT. F: Body weight of WT→WT and KD→WT mice fed an ND or HFD for 15 weeks. G: ITT and GTT determined after 15 weeks of ND or HFD feeding. H: Serum insulin, glucose, adiponectin, cholesterol, free fatty acid, and triglyceride levels in ND- or HFD-fed WT→WT and KD→WT mice. I: Energy expenditure of WT→WT and KD→WT mice. vO₂ consumption was measured in the dark and light phases as described in RESEARCH DESIGN AND METHODS (WT: n = 6; KD: n = 6). J: Food intake was monitored and normalized to body weight. For B–J, Student test was used and presented as mean ± SD. Experiments were performed two times. *P < 0.05; **P < 0.01; ***P < 0.001.

Decrease in M1 and Increase in M2 ATMs in HFD-Fed MφRIP140KD Mice

As described above, MφRIP140KD mice show vWAT browning and an improved metabolic profile even after a long-term HFD feeding. To determine how an HFD might impact on various cell populations in the SVF of vWAT, we analyzed leukocyte populations. As predicted, all immune cells in WT mice, including macrophages, neutrophils, eosinophils, and T and B lymphocytes are increased under HFD as compared with ND (Supplementary Fig. 5). HFD-fed MφRIP140KD mice have a significant increase only in their macrophage population (Fig. 4A, left), but not neutrophils, eosinophils, or T or B lymphocytes (Supplementary Fig. 5). Importantly, M1 expansion (Fig. 4A, middle) occurs to a lesser degree, and the M2 population is increased (Fig. 4A, right) in MφRIP140KD mice, suggesting that typical HFD-induced M1 expansion (mostly from recruitment) in vWAT is reduced in MφRIP140KD mice.

We subsequently validated the gene expression profiles of SVF from vWAT. In WT mice, all of the examined M1 markers (Cd11c, Il1β, Il6, Nos2, and Tnfα) in the ATM of vWAT are dramatically elevated under an HFD, whereas such elevation is almost entirely abolished in the vWAT of MφRIP140KD mice (Fig. 4B). Moreover, in MφRIP140KD mice, all of the examined M2 markers (Arg1, Il10, Mgl1 [Cd301], Mgl2, Mrc1 [Cd206], and Mrc2) are already significantly elevated under ND, and most of these M2

markers become even further elevated upon HFD feeding (Fig. 4C). These data confirm that lowering the RIP140 level in macrophages reduces the inflammatory population and increases the anti-inflammatory population. Together, changes in ATM populations could contribute to the reduction in HFD-induced adipose inflammation.

Decreased Circulating Proinflammatory Monocytes and M1 Recruitment in ATM of HFD-Fed MφRIP140KD Mice

We analyzed the numbers of circulating $CD115^+Ly6C^+$ (proinflammatory) and/or $Ly6C^-$ (anti-inflammatory) monocytes in WT and MφRIP140KD mice using FACS (gating strategy provided in Supplementary Fig. 6). As shown in Fig. 5A, left, $CD115^+Ly6C^+$ and $Ly6C^-$ circulating monocyte populations are comparable between WT and KD under an ND. But under an HFD, the $CD115^+Ly6C^+$ inflammatory monocyte number is higher in WT mice as compared with MφRIP140KD mice. By contrast, the $CD115^+Ly6C^-$ anti-inflammatory monocyte number is higher in MφRIP140KD mice as compared with WT mice (Fig. 5A, right). The results demonstrate that lowering the RIP140 level in the monocyte/macrophage lineage affects the blood monocyte populations by reducing inflammatory monocytes, especially under HFD. ATMs are originally derived from BM and differentiated in AT from infiltrated monocytes (28). Previous results (Fig. 4A) indicate that ATM infiltration in vWAT is decreased in
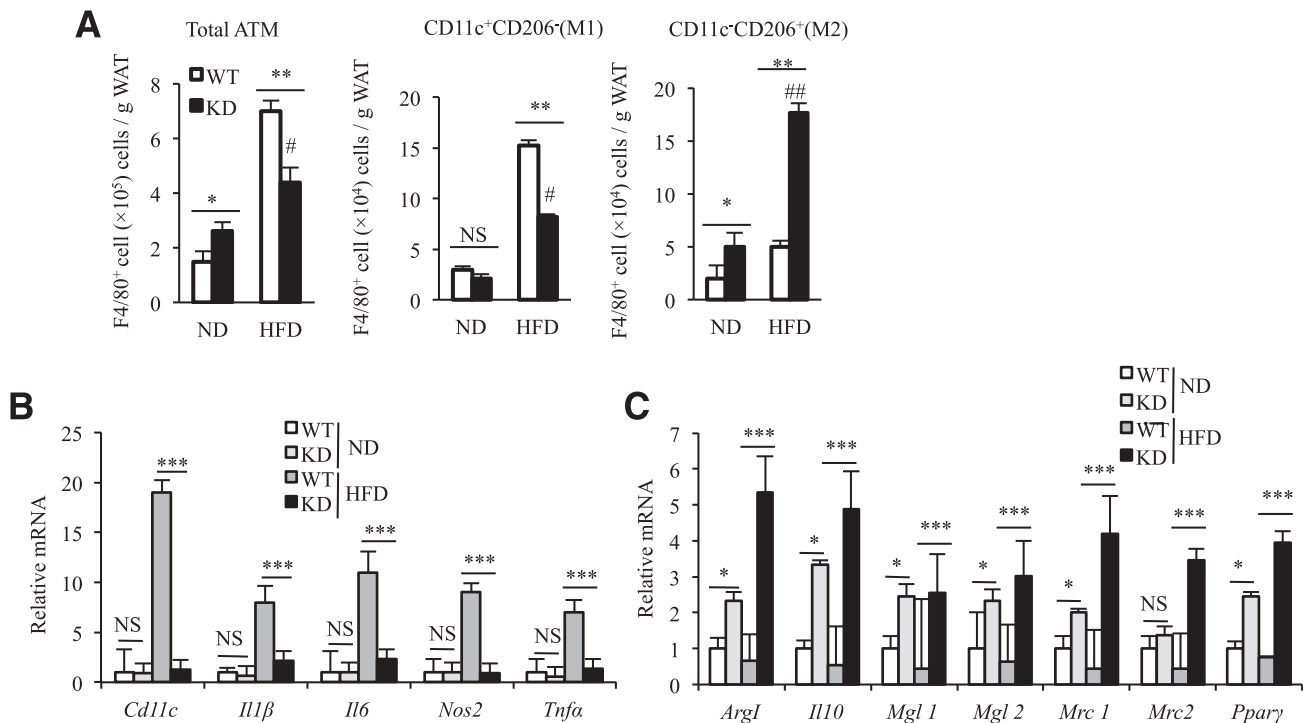

Figure 4—Decreased total ATM and altered M1/M2 profile in the vWAT of MφRIP140KD mice. A: FACS evaluation of ATM population of the SVF in vWAT. The statistic results show the ATM population and M1/M2 distribution in vWAT of WT and KD, under ND or HFD, that is normalized to the vWAT mass. The analyzed cells are from the SVF as shown in Supplementary Fig. 5A. B and C: qPCR determining mRNA levels in the SVF of vWAT. Student test was used and presented as mean ± SD. n = 5 to 6 mice/group. All experiments were performed two times. #P < 0.05 and ##P < 0.01 for comparison of ND-RIP140 mice with HFD-RIP140 KD mice. *P < 0.05; **P < 0.01; ***P < 0.001.
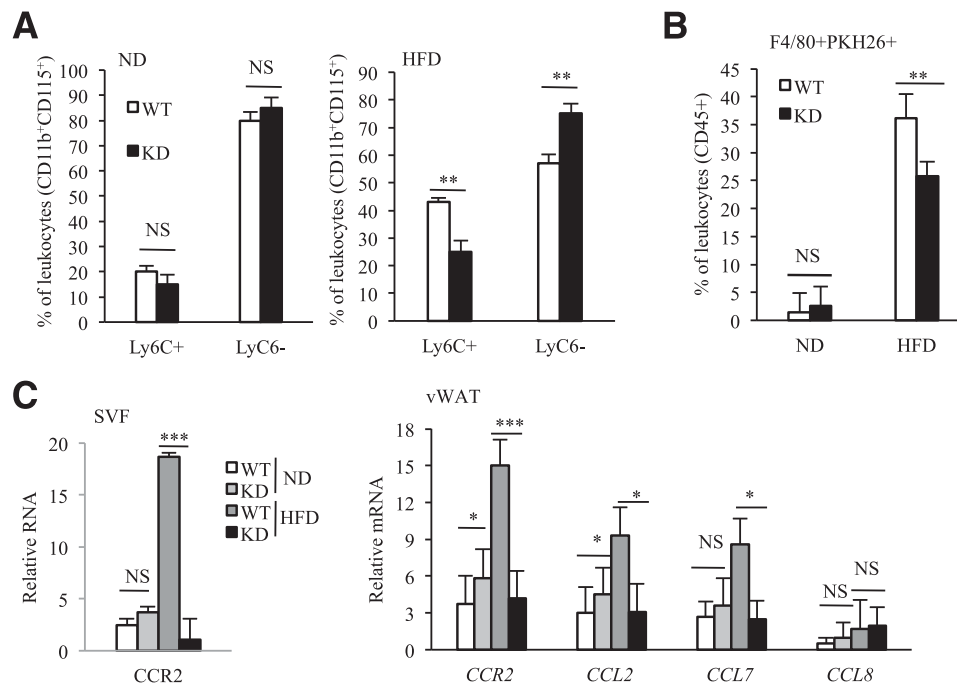
Figure 5—Monocyte and macrophage recruitment. *A*: Quantification of circulating CD115⁺Ly6C⁺ (proinflammatory) and/or Ly6C⁻ (anti-inflammatory) monocyte analyzed by FACS. *B*: Quantification of F4/80⁺PKH26⁺ (indicative of recruited ATM) in vWAT analyzed by FACS. *C*: qPCR analyses of mRNAs of chemokines and their cognate receptors in the SVF or total vWAT. Data are presented as mean ± SD; n = 4 mice/group and Student test was used. Data were performed in duplicate. *P < 0.05; **P < 0.01; ***P < 0.001.

HFD-fed MφRIP140KD mice. We thus examined whether RIP140 affects ATM dynamics also because of reduced monocyte recruitment. To directly monitor the infiltration of monocyte/macrophage into vWAT, we transferred PKH26-labeled BM (ATM progenitor) cells from WT and Mφ-RIP140KD mice into normal mice and followed the distribution of these labeled cells in the vWAT of recipient mice after HFD. Supplementary Fig. 7 depicts the experimental design and FACS data. Statistical analyses are shown in Fig. 5*B*. Under an ND, the recruitment of all PKH26-labeled ATMs is relatively constant (1.5% in WT and 2.6% in MφRIP140KD mice); but after an HFD, recruitment is significantly altered: 36.2% in WT and 25.8% in MφRIP140KD mice. This is consistent with the difference in the ATM profile between WT and MφRIP140KD (Fig. 4*A*). We then examined changes in the expression patterns of key cytokine receptors in the SVF and vWAT fraction. As expected, M1-specific CCR2 and its chemokine ligands are elevated in HFD-fed WT mice, but the elevation of these M1 molecular markers is significantly reduced in MφRIP140KD mice (Fig. 5*C*), supporting that HFD-induced recruitment of M1 state ATMs is also retarded in MφRIP140KD mice. These data are consistent with the reduction of proinflammatory M1 ATM in HFD-fed MφRIP140KD mice.

DISCUSSION

Obesity-induced chronic inflammation is critical in the pathogenesis of IR and other metabolic diseases (29). A

significant advance in our understanding of obesity-associated inflammation and IR is the recognition of the critical role of ATMs (7). Evidence has accumulated that in obese mice and humans, there is an increase in M1 ATMs and decrease in M2 ATMs. In this study, we found that RIP140 expression is increased in ATMs of HFD-fed mice, and it plays an important role in regulating HFD-induced monocyte and ATM polarization that contributes to AT inflammation.

It has been reported that cold stress or IL-4 can enhance M2 in BAT and WAT (27). In WAT, M2 releases catecholamines to enhance lipolysis, which provides fuel to BAT for thermogenesis. Studies have suggested that converting white adipocytes into brown or brownlike (beige) adipocytes in WAT (stimulating WAT browning) can be a useful strategy in managing obesity and IR. In this study, we uncover a function of RIP140 in ATMs to regulate adipocyte phenotype. Reducing RIP140 results in fewer M1 and more M2, which is beneficial to adipose tissue remodeling and improves its anti-inflammatory status, particularly under an HFD feeding. Our data also provide evidence that it is possible to enhance browning of WAT, even under an HFD feeding, by lowering RIP140 to reduce M1 and increase M2 polarization in ATMs, which improves insulin sensitivity. How RIP140 KD macrophage stimulates the browning of WAT remains to be elucidated. To this end, we detected browning effects caused directly by CM of MφRIP140KD macrophages and elevation in catecholamine-synthesizing rate-limiting enzyme, TH, in MφRIP140KD animal's ATMs. We also found that RIP140KD could enhance the

expression of TH in IL-4–stimulated macrophages. RIP140 may regulate TH expression in macrophages, thereby modulating catecholamine production to affect vWAT browning. A recent study (21) showed ablating RIP140 in adipocytes stimulated browning, suggesting cell-autonomous repressive activity of RIP140 in the browning program of adipocytes. Our study indicates RIP140 also plays a negative role in adipose tissue browning through its action in ATMs. Accordingly, it is tempting to speculate that RIP140 can be a negative, physiological regulator of AT browning.

Recent studies indicated that ATM arises from a lineage that includes BM precursors and blood monocytes (28). M1 ATM increases by recruiting a population of Ly6C$^+$ monocytes through CCR2–CCL2 signaling (30). Our data support this idea. We observed that reducing RIP140 more significantly affects Ly6C$^+$ circulating monocyte population and inhibits the M1-type ATM recruitment in AT. In mice, Ly6C$^+$ monocytes accumulate in AT and elicit inflammation (31), whereas Ly6C$^-$ monocytes participate in resolving inflammation (32). A predominance of the Ly6C$^-$ over Ly6C$^+$ monocyte population was observed in the peripheral blood of HFD-fed MφRIP140 KD mice (Fig. 5A). The alteration of Ly6C$^+$ and Ly6C$^-$ circulating monocyte subsets could contribute to the M2-dominant shift of ATMs in HFD-fed MφRIP140 KD mice. M2 ATMs could proliferate in situ during obesity-inducing inflammation (33). Although Ly6C$^-$ monocytes have been suggested to give rise to M2 macrophages, this relationship has not been firmly established (34). The dramatic reduction in M1 by lowering RIP140 levels with a relative increase in M2 would contribute to the overall dynamic changes in ATM populations seen in MφRIP140 KD mice. However, studies are required to determine whether and how lowering RIP140 may also enhance the M2-dominant shift.

In our previous studies, we showed that regulating RIP140 levels in macrophages controls the inflammatory response, including endotoxin tolerance (22) and septic shock (17). Under HFD feeding, although circulating monocyte/macrophage numbers are decreased in RIP140KD mice as compared with WT mice, RIP140KD mice in fact harvest fewer Ly6C$^+$ proinflammatory monocytes, but more Ly6C$^-$ anti-inflammatory monocytes. Overall, it may be concluded that downregulating RIP140 in macrophages will reduce proinflammation and increase anti-inflammation. However, responses of these animals to various infectious agents remain to be examined.

In conclusion, RIP140 is involved in regulating monocyte and ATM homeostasis. Reducing RIP140 correlates with attenuation in circulating M1 and reduction in M1 recruitment to ATMs. The dynamic changes in these important innate immune cell populations impact the overall polarization pattern of ATMs in fat tissues. This particular ATM phenotype is beneficial to the browning in vWAT and the improved metabolic phenotype of these animals.

Author Contributions. P.-S.L. and Y.-W.L. designed the experiments, analyzed the data, and performed the experiments. B.L., S.K.M.-S., and J.A.L. performed the experiments. L.-N.W. designed the experiments, analyzed the data, and provided financial support. L.-N.W. is the guarantor of this work and, as such, had full access to all the data in the study and takes responsibility for the integrity of the data and the accuracy of the data analysis.

References

1. Mosser DM, Edwards JP. Exploring the full spectrum of macrophage activation. Nat Rev Immunol 2008;8:958–969

2. Lawrence T, Natoli G. Transcriptional regulation of macrophage polarization: enabling diversity with identity. Nat Rev Immunol 2011;11:750–761

3. Ivashkiv LB. Epigenetic regulation of macrophage polarization and function. Trends Immunol 2013;34:216–223

4. Gautier EL, Shay T, Miller J, et al.; Immunological Genome Consortium. Gene-expression profiles and transcriptional regulatory pathways that underlie the identity and diversity of mouse tissue macrophages. Nat Immunol 2012;13: 1118–1128

5. Lumeng CN, Bodzin JL, Saltiel AR. Obesity induces a phenotypic switch in adipose tissue macrophage polarization. J Clin Invest 2007;117:175–184

6. Odegaard JI, Chawla A. Alternative macrophage activation and metabolism. Annu Rev Pathol 2011;6:275–297

7. Wynn TA, Chawla A, Pollard JW. Macrophage biology in development, homeostasis and disease. Nature 2013;496:445–455

8. Chawla A, Nguyen KD, Goh YP. Macrophage-mediated inflammation in metabolic disease. Nat Rev Immunol 2011;11:738–749

9. Lumeng CN, DelProposto JB, Westcott DJ, Saltiel AR. Phenotypic switching of adipose tissue macrophages with obesity is generated by spatiotemporal differences in macrophage subtypes. Diabetes 2008;57:3239–3246

10. Mantovani A, Sica A, Sozzani S, Allavena P, Vecchi A, Locati M. The chemokine system in diverse forms of macrophage activation and polarization. Trends Immunol 2004;25:677–686

11. Gordon S, Taylor PR. Monocyte and macrophage heterogeneity. Nat Rev Immunol 2005;5:953–964

12. Geissmann F, Jung S, Littman DR. Blood monocytes consist of two principal subsets with distinct migratory properties. Immunity 2003;19:71–82

13. Dalmas E, Clément K, Guerre-Millo M. Defining macrophage phenotype and function in adipose tissue. Trends Immunol 2011;32:307–314

14. Ho PC, Wei LN. Biological activities of receptor-interacting protein 140 in adipocytes and metabolic diseases. Curr Diabetes Rev 2012;8:452–457

15. White R, Leonardsson G, Rosewell I, Ann Jacobs M, Milligan S, Parker M. The nuclear receptor co-repressor nrip1 (RIP140) is essential for female fertility. Nat Med 2000;6:1368–1374

16. Mostaqul Huq MD, Gupta P, Tsai NP, White R, Parker MG, Wei LN. Suppression of receptor interacting protein 140 repressive activity by protein arginine methylation. EMBO J 2006;25:5094–5104

17. Ho PC, Chang KC, Chuang YS, Wei LN. Cholesterol regulation of receptor-interacting protein 140 via microRNA-33 in inflammatory cytokine production. FASEB J 2011;25:1758–1766

18. Wei LN. Chromatin remodeling and epigenetic regulation of the Crabpl gene in adipocyte differentiation. Biochim Biophys Acta 2012;1821:206–212

19. Ho PC, Lin YW, Tsui YC, Gupta P, Wei LN. A negative regulatory pathway of GLUT4 trafficking in adipocyte: new function of RIP140 in the cytoplasm via AS160. Cell Metab 2009;10:516–523

20. Ho PC, Chuang YS, Hung CH, Wei LN. Cytoplasmic receptor-interacting protein 140 (RIP140) interacts with perilipin to regulate lipolysis. Cell Signal 2011;23:1396–1403

21. Kiskinis E, Chatzeli L, Curry E, et al. RIP140 represses the "brown-in-white" adipocyte program including a futile cycle of triacylglycerol breakdown and synthesis. Mol Endocrinol 2014;28:344–356

22. Zschiedrich I, Hardeland U, Krones-Herzig A, et al. Coactivator function of RIP140 for NFkappaB/RelA-dependent cytokine gene expression. Blood 2008; 112:264–276

23. Ho PC, Tsui YC, Feng X, Greaves DR, Wei LN. NF-κB-mediated degradation of the coactivator RIP140 regulates inflammatory responses and contributes to endotoxin tolerance. Nat Immunol 2012;13:379–386

24. Gough PJ, Gordon S, Greaves DR. The use of human CD68 transcriptional regulatory sequences to direct high-level expression of class A scavenger receptor in macrophages in vitro and in vivo. Immunology 2001;103:351–361

25. Seale P, Conroe HM, Estall J, et al. Prdm16 determines the thermogenic program of subcutaneous white adipose tissue in mice. J Clin Invest 2011;121:96–105

26. Wu J, Boström P, Sparks LM, et al. Beige adipocytes are a distinct type of thermogenic fat cell in mouse and human. Cell 2012;150:366–376

27. Nguyen KD, Qiu Y, Cui X, et al. Alternatively activated macrophages produce catecholamines to sustain adaptive thermogenesis. Nature 2011;480:104–108

28. Weisberg SP, McCann D, Desai M, Rosenbaum M, Leibel RL, Ferrante AW Jr. Obesity is associated with macrophage accumulation in adipose tissue. J Clin Invest 2003;112:1796–1808

29. Hotamisligil GS. Inflammation and metabolic disorders. Nature 2006;444: 860–867

30. Oh DY, Morinaga H, Talukdar S, Bae EJ, Olefsky JM. Increased macrophage migration into adipose tissue in obese mice. Diabetes 2012;61:346–354

31. Tsou CL, Peters W, Si Y, et al. Critical roles for CCR2 and MCP-3 in monocyte mobilization from bone marrow and recruitment to inflammatory sites. J Clin Invest 2007;117:902–909

32. Auffray C, Fogg D, Garfa M, et al. Monitoring of blood vessels and tissues by a population of monocytes with patrolling behavior. Science 2007;317:666–670

33. Amano SU, Cohen JL, Vangala P, et al. Local proliferation of macrophages contributes to obesity-associated adipose tissue inflammation. Cell Metab 2014; 19:162–171

34. Bouhlel MA, Derudas B, Rigamonti E, et al. PPARgamma activation primes human monocytes into alternative M2 macrophages with anti-inflammatory properties. Cell Metab 2007;6:137–143